Numerical model of rapidly solidified droplets of Al-33wt%Cu eutectic growth

J. Valloton[1], A-A. Bogno[1], M. Rappaz[2], H. Henein[1]

1- Advanced Materials and Processing Laboratory, Department of Chemical and Materials Engineering, University of Alberta, Edmonton, Alberta, T6G 1H9, Canada
Email Address: valloton@ualberta.ca

2- Ecole Polytechnique Fédérale de Lausanne, Institute of Materials, 1015 Lausanne, Switzerland

---

Abstract: Rapid solidification of Al-Cu droplets of eutectic composition was carried out using Impulse Atomization (a type of drop tube). Two distinct morphologies were observed: an irregular undulated eutectic assumed to form during recalescence, followed by a regular lamellar eutectic. The volume fraction of each morphology was measured and used to deduce the nucleation undercooling based on the hypercooling limit. A model of the eutectic solidification was developed assuming that the kinetics of the undulated and regular regions is the same and follows scaling laws established experimentally. The simulated solid fraction forming during recalescence matches the experimental undulated eutectic fraction. Furthermore, the heat balance confirms the adiabatic nature of the solidification during recalescence. Good agreement is found between the model and experimental measurements of lamellar spacing for the regular eutectic. However, the predicted spacing of the undulated eutectic is much lower than what is observed experimentally. This difference as well as the nature of this morphology is attributed to coarsening during the remaining of solidification of the very fine eutectic formed during recalescence.

Keywords: rapid solidification, Al-Cu, eutectic, lamellar spacing, heat transfer, modeling

---

1. Introduction

High undercoolings and cooling rates associated with rapid solidification of metallic alloys result in various beneficial microstructural features, such as minimal segregation, grain refinement, solubility extension and the formation of metastable phases. Therefore, it is important to understand the relationship between the microstructures and the solidification parameters in order to control their solidification path and subsequent mechanical properties. However, it is sometimes difficult to relate the observed microstructure with process parameters due to experimental difficulties. These include measurements of variables such as cooling rate, undercooling and solidification rate, which control the final solidification microstructure. Thus, to understand the phenomena at play, rapid solidification experiments with controlled solidification parameters are helpful. Impulse Atomization (IA) is a rapid solidification technique that yields droplet forming with high levels of undercooling over a wide range of cooling rates

[1]–[4]. It also provides a reliable and reproducible thermal history for the cooling droplets making quantitative analysis feasible.

Eutectic alloys are very attractive due to their good fluidity allowing ready shaping of parts in casting processes as well as in thermal spray deposition. In addition, they yield microstructures with high mechanical properties, by the virtue of their scale, which is defined by the solidification parameters as well as the thermodynamic and thermophysical properties of the given alloy. Al-Cu is one of the simplest binary eutectic systems, with a well-documented phase diagram and physical constants. Its growth kinetics is also well-established, with a relationship between the eutectic front velocity v^* and the interlamellar spacing λ given by the equation $\lambda^2 v^*$ = constant [5].

Modeling of cooling and solidification of molten metal droplets during atomization requires an understanding of the thermal exchange between a droplet and a surrounding gas medium [6]. Of particular importance is the determination of the heat transfer coefficient. The most common approach to quantify this coefficient is through the use of semi-empirical equations in which the Nusselt number is averaged over the entire droplet surface. Several correlations have been proposed for that purpose [7]–[13]. The Ranz-Marshall [9] and Whitaker [10] correlations are the most commonly used, even though the range of validity in which these correlations were derived is often exceeded in atomization of molten metals. Uncertainties also remain regarding the temperature at which the thermophysical properties of gas should be evaluated, i.e. at the gas free stream temperature or at the film temperature.

This paper presents experimental results of Al-33wt%Cu droplets rapidly solidified using Impulse Atomization. A model of the eutectic growth is developed and coupled to a transient heat flow model of IA. The modelling results are then validated with experimental measurements of the lamellar spacing to determine which correlation is most appropriate.

2. Experiments

Impulse atomization (IA) (a type of drop tube) is a containerless solidification technique (Figure 1) [1]. It consists in the transformation of a bulk liquid into a spray of liquid droplets of fairly uniform size. In this study, a quantity of 300g of high purity Al (99.99%) and commercial purity Cu (99.9%) is melted in a dense graphite crucible by induction heating up to 750°C (~ 200°C above the equilibrium eutectic temperature) and held for 1 hour under argon atmosphere. A plunger (or impulse applicator) applies a pressure (or impulse) to the melt in order to push it through a nozzle plate with several orifices of known size and geometry. Liquid ligaments emanate from each orifice, which in turn break up into droplets by Rayleigh instability. Rapid solidification of the droplets then occurs during free fall by heat loss to the surrounding gas (Ar in this case). The solidified samples can finally be collected at the bottom of the tower and subsequently sieved into different size classes. A detailed description of the process is available

in [1]. Powders of select size ranges were then densely packed and cold-mounted in epoxy and ground. The samples were then polished until the mounted droplets were nearly touching each other to ensure that the cross-sections were as close to the mid-section of the particles as possible. Imaging was performed using a Tescan Vega-3 SEM in back-scattered mode. Lamellar spacing as a function of position within the droplet was determined using a line-intercept method along arc of circles (see below).

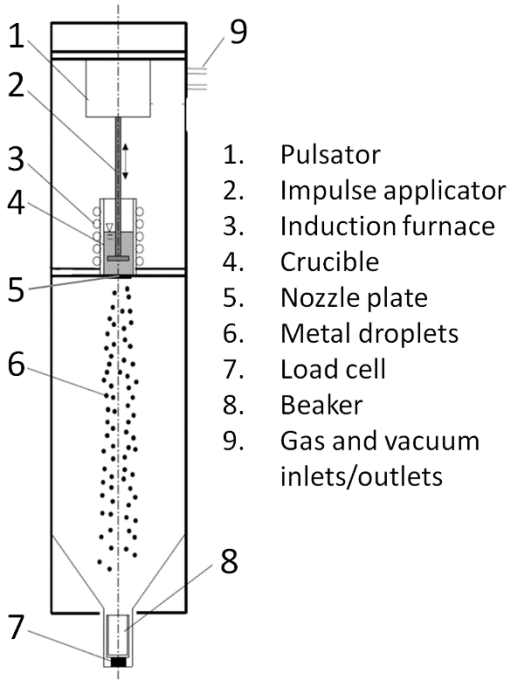

Figure 1: Schematic view of an impulse atomization apparatus [1].

Figure 2a shows the typical microstructure of undercooled Al33Cu droplets. Two different eutectic morphologies can clearly be observed: an undulated eutectic (zone A) followed by a transition to a regular lamellar eutectic (zone B). From the fan-shape of the morphology, it is obvious that nucleation started from the center of symmetry in zone A at the surface of the droplet (marked by point "N"). A detailed view of the eutectic structure at the transition between zones A and B is shown in Figure 2b, with two inserts showing details of both structures (Figures 2c and 2d). Please note that lamellae of the regular eutectic might appear with different Moiré patterns in 2D sections (stereological aspects)

While this assumption will be further discussed later, it is assumed that the undulated eutectic forms during the nearly adiabatic recalescence, while the regular eutectic grows during solidification controlled by the heat exchange with the surrounding gas (Figure 3 left). After nucleation occurs at an undercooling ΔT_n, the eutectic front indeed rapidly propagates through the volume of the droplet. The release of the latent heat of solidification leads to a rapid increase of the droplet temperature. The undercooled melt acts as a heat sink and due to rapid

crystallization the heat transfer to the environment can be neglected, as demonstrated hereafter. Under quasi-adiabatic solidification conditions, the nucleation undercooling ΔT_n can therefore be estimated from the volume fraction g_A of Zone A and the hypercooling limit of the melt, ΔT_{hyp}:

$$\Delta T_n = g_A \,.\, \Delta T_{hyp} = g_A \,.\, \frac{L_f}{c_p} \qquad (1)$$

with L_f is the latent heat of fusion and c_p the heat capacity.

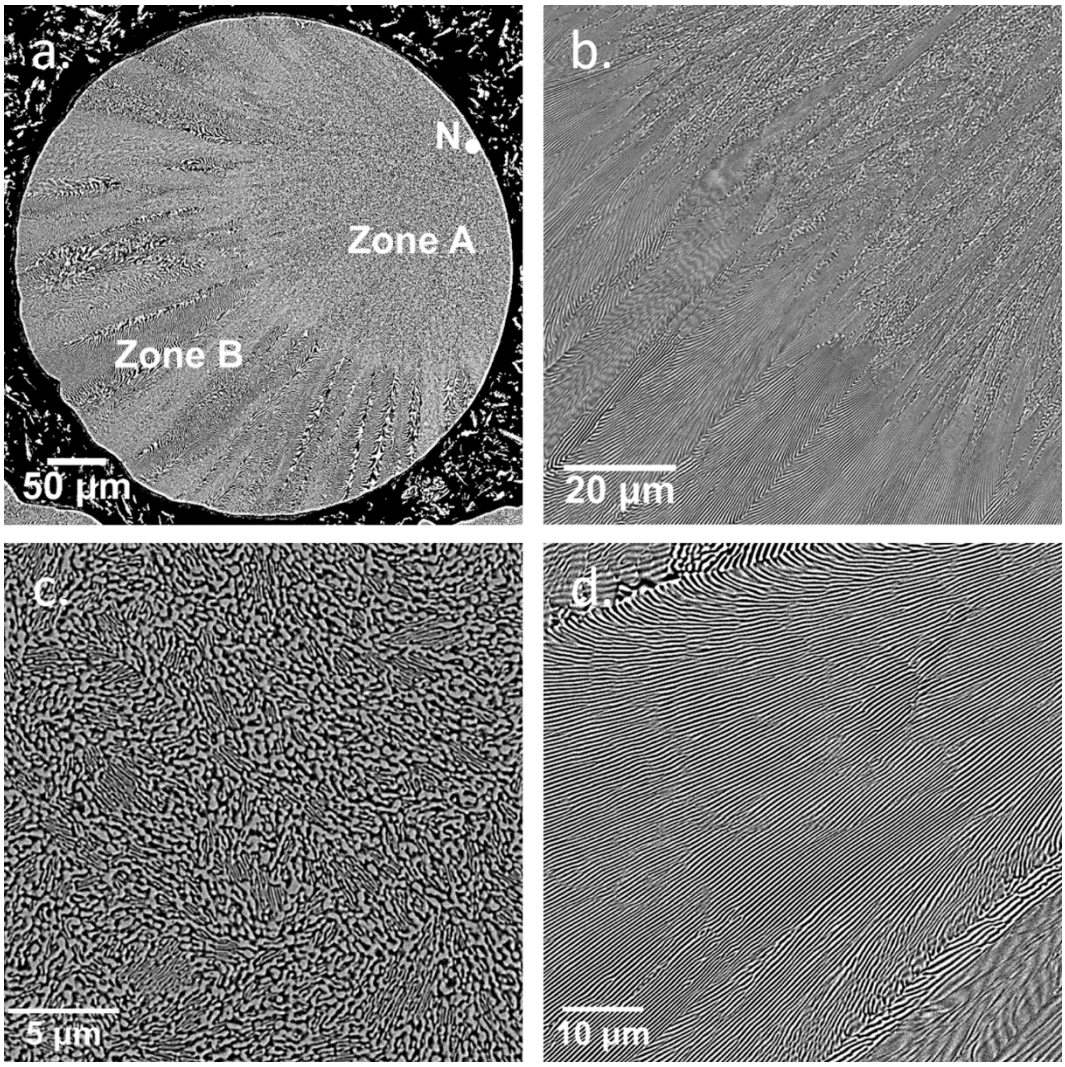

Figure 2: a: Microstructure of a 425 µm droplet atomized in Ar showing the undulated and regular eutectic structures (Zones A and B, respectively). From the volume fraction of these zones, the undercooling ΔT_n is estimated to be 85 K in this case. b: Close-up of the transition between zones A and B. c: Close-up of zone A. d: Close-up of zone B.

Figure 3 (right) shows the estimated nucleation undercoolings of 13 particles of different sizes. The undercooling tends to decrease as the particle size increases and conversely when the

cooling rate decreases. This is consistent with previous studies on Impulse Atomized Al-4.5wt%Cu and Al-10wt%Si droplets [3], [4]. However, nucleation being a stochastic event, some scatter in the undercooling data can be observed. More measurements are needed to obtain better statistics and confirm this trend.

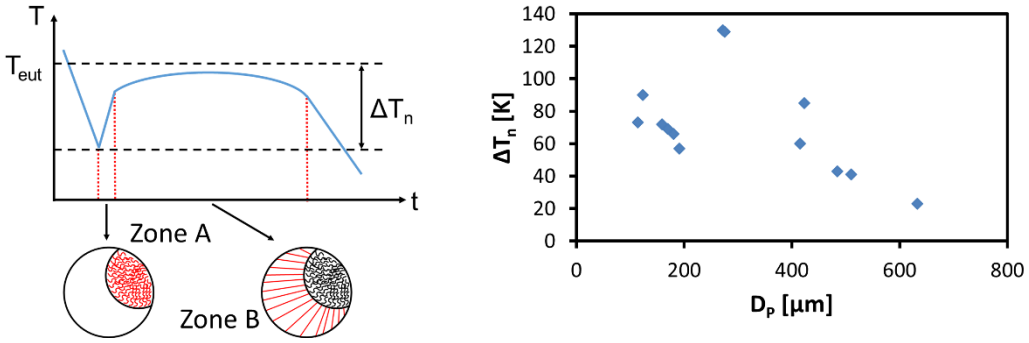

Figure 3: Left: Schematic temperature profile. Right: Nucleation undercooling as a function of the particle diameter D_P estimated from the fraction of undulated eutectic (Eq. 1).

3. Model

Assuming heat diffusion in the metal to be very fast, the model considers that the temperature *T* of the droplet is uniform (this will be verified below). Under such hypothesis, a simple heat balance equation can be written:

$$-h_{ext}(T - T_{ext})4\pi R_P^2 = \rho c_p \frac{4}{3}\pi R_P^3 \frac{dT}{dt} - \rho L_f \frac{dV_s}{dt} \quad (2)$$

where h_{ext} is the effective heat transfer coefficient between the droplet and the surrounding gas, T_{ext} is the atomization gas temperature, ρ, c_p , L_f and R_P are the particle density, heat capacity, latent heat of fusion and radius, respectively. V_s is the volume of the solidified eutectic. The thermal history of the liquid droplet is a function of both the droplet size and the gas in the atomization tower and has been described mathematically by previous workers [2] [3]. After reaching a nucleation undercooling (estimated from experiments), the eutectic front grows with a spherical envelope from the nucleation point located at the surface of the droplet (see Figure 4).

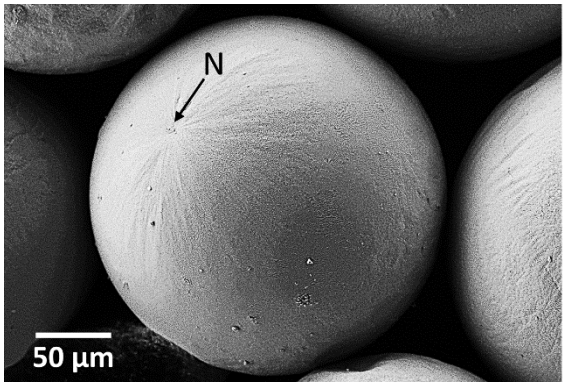

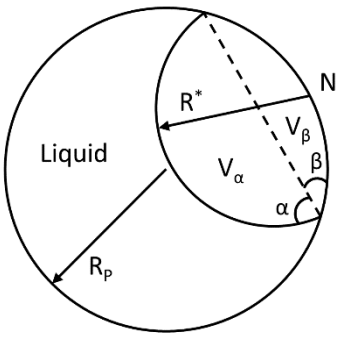

$$V_s(R^*) = V_\alpha(R^*) + V_\beta(R^*)$$

Figure 4: Left: Surface of a 230 µm Al33Cu droplet viewed in SEM. The arrow indicates the location of the nucleation point N. Right: Schematic view of the spherical eutectic growth front.

The relationship between the volume V_s and the radius R^* of the solid already formed is deduced by decomposing V_s into two spherical caps V_α and V_β of radii R^* and R_p, respectively, as indicated in Figure 4. This decomposition allows also to calculate the effective solid-liquid interface S_{sl} and thus to relate the evolution of the fraction of solid, $\frac{dV_s}{dt} = S_{sl}v^*$, appearing in Eq. (2) to the actual velocity of the interface $v^* = \frac{dR^*}{dt}$. These relationships are given in Appendix A.

The effective heat transfer coefficient consists of the additive contributions of convection, conduction and radiation heat transfer mechanisms. h_{ext} is defined as:

$$h_{ext} = h_c + h_{rad} \tag{3}$$

with h_{rad} the radiative, and h_c the convective and conductive components of the heat transfer coefficient. The radiative heat transfer coefficient is readily characterized as:

$$h_{rad} = \varepsilon\sigma(T_0^2 + T_s^2)(T_0 + T_s) \tag{4}$$

with ε the emissivity, σ the Stefan-Boltzmann constant, T_s the surface temperature of the droplet and T_0 the temperature of the surrounding (assumed to be equal to that of the gas far from the droplet). The convective/conductive heat transfer component can be calculated using the Nusselt number averaged over the entire droplet surface [14]:

$$Nu = \frac{h_c D_P}{k_g} \tag{5}$$

with D_P the diameter of the particle and k_g the conductivity of the surrounding atomization gas. Two common semi-empirical correlations are used to evaluate Nu. The first one was proposed by Ranz and Marshall [9]:

$$Nu_{RM} = 2 + 0.6Re^{1/2}Pr^{1/3} \quad (6)$$

with $Re = \frac{\rho_g v D_P}{\mu_g}$ the Reynolds number and $Pr = \frac{c_{p,g}\mu_g}{k_g}$ the Prandtl number. ρ_g, μ_g and $c_{p,g}$ are the density, dynamic viscosity and heat capacity of the gas, respectively. The second correlation is that of Whitaker [10]:

$$Nu_W = 2 + (0.4Re^{1/2} + 0.006Re^{2/3})Pr^{0.4}\left(\frac{\mu_\infty}{\mu_s}\right)^{1/4} \quad (7)$$

where $\frac{\mu_\infty}{\mu_s}$ is the ratio between the dynamic gas viscosities at the free stream gas temperature, μ_∞, and at the droplet surface temperature, μ_s. For each correlation, two cases were considered for the calculation of the Reynolds and Prandlt numbers. In the first case, all gas properties were taken at the ambient temperature, T_0. In the second case, gas properties were taken at the film temperature, $T_{film} = (T_0 + T_s)/2$, i.e. the average between the ambient T_0 and the droplet surface temperature T_s. The thermophysical properties of Al-33wt%Cu (considered constant and equal for solid and liquid) and argon used in this work are listed in Table 1 and 2 respectively.

Table 1: Thermophysical properties of Al-33wt%Cu [16]

Property	**Symbol**	**Al-33wt%Cu**
Density [kg/m^3]	ρ	3700
Specific heat [J/kg·K]	c_p	773
Latent heat of fusion [J/kg]	L_f	3.32×10^5
Conductivity [W/m·K]	k	125

Table 2: Thermophysical properties of argon [17]–[19]

Property (T in K)	**Symbol**	**Argon**
Density [kg/m^3]	ρ_g	$539.23\cdot T^{-1.0205}$
Specific heat [J/kg·K]	$c_{p,g}$	520
Dynamic viscosity [Pa·s]	μ_g	$0.0238\cdot T^{0.7913}\cdot10^{-5}$
Conductivity [W/m·K]	k_g	$1.86\cdot T^{0.7915}\cdot10^{-4}$

Knowing the heat transfer coefficient allows the computation of the Biot number:

$$Bi = \frac{h_{ext}D_P}{k} \sim \frac{T_c - T_s}{T_s - T_0} \quad (8)$$

where k is the thermal conductivity of the alloy. For the smallest and largest sizes analyzed (10 µm droplet, experiencing the highest cooling rate, and 1000 µm droplet, experiencing the

lowest cooling rate), h_{ext} is in the order of 4000 and 100 W/m^2·K respectively. This results in Biot numbers of $3\cdot10^{-4}$ and $8\cdot10^{-4}$ << 0.1. At the eutectic temperature, this corresponds to a temperature difference ($T_c - T_s$) between the center and the surface of the droplet of less than 0.5 K. Thus, the temperature of the droplets can indeed be considered to be nearly uniform.

The only missing entity appearing in Eq. (2) is the growth kinetics of the eutectic $v^*(T)$, since $\frac{dV_s}{dt} = S_{sl}\, v^*(T)$ and S_{sl} is a known function of the radius R^* (see Appendix). The growth kinetics is determined using established scaling laws for regular eutectics such as Al-Al_2Cu [20], [21]:

$$A_C = \frac{\Delta C_o}{g_\alpha g_\theta} \frac{|m_\alpha||m_\theta|}{(|m_\alpha|+|m_\theta|)} \sum \frac{sin^2(n\pi g_\alpha)}{(n\pi)^3} \tag{9}$$

$$\lambda^2 v^* = \frac{A_R}{A_C} D_l = 88\ [\mu m^3 s^{-1}] \tag{10}$$

$$\lambda \Delta T = 2A_R \tag{11}$$

The various terms appearing in these equations are: the diffusion growth constant A_C for Cu in the liquid, the capillary growth constant A_R, the spacing λ of the (α-Al)-Al_2Cu eutectic lamellae, the undercooling of the eutectic front $\Delta T = (T_{eut} - T)$, and the solute extension at the eutectic plateau ΔC_o. The subscripts α and θ refer to the α-Al solid solution and the Al_2Cu intermetallic, respectively.

The volume fractions of α and θ, g_α and g_θ, are taken from a lever rule at the equilibrium eutectic temperature. The liquidus slopes m_α and m_θ appearing also in the definition of A_C (Eq. 9) are obtained using Thermo-Calc (TTAL7 database). They are computed at various undercoolings during the calculation from the extensions of the liquidus lines below the eutectic temperature. The diffusion coefficient of Cu in the liquid, D_l, is temperature-dependent and given by [18]:

$$D_l = 1.05 \cdot 10^{-7} e^{\frac{23800}{RT}}\ [m^2 s^{-1}] \tag{12}$$

As A_C and D_l are known, the capillary growth constant A_R, which is difficult to estimate as it is related to the poorly known surface tensions of α and θ, is calculated from the experimentally determined relationship (10).

In a time-stepping calculation where the actual temperature of the droplet $T(t)$ is known, the liquid diffusion coefficient D_l and the eutectic coefficient A_C are first computed. A_R is then inferred from Eq. (10). The lamellar spacing λ and growth velocity v^* are then calculated as a function of the undercooling from Eqs. (10) and (11). The change in the volume fraction of solid $\frac{dV_s}{dt}$ is then inferred from the new solid radius $R^*(t+dt) = R^*(t) + v^* dt$. The heat balance equation (1) is finally solved explicitly to obtain the new droplet temperature $T(t+dt)$.

4. Results and discussion

Figure 5 shows an SEM cross-section of a 123 µm diameter droplet. The white dot indicates the center of zone A, i.e. the nucleation point. The radius of zone A (as highlighted by the white circle) is 52.3 µm. This represents a volume fraction $g_A \approx 0.21$, corresponding to an undercooling ΔT_n of about 90 K. The left graph shows the simulated temperature profiles using the Whitaker (black) and Ranz-Marshall (blue) correlations with thermophysical properties of the atomization gas taken at the ambient temperature (solid) and at the film temperature (dashed). For a given set of gas properties, the Ranz-Marshall correlation leads to higher cooling rates and shorter solidification times than the Whitaker one. The predicted cooling rates also increase when the thermophysical properties are taken at the film temperature rather than at the ambient gas temperature. This directly affects the solidification behaviour of the lamellar eutectic.

The graph on the right shows the simulated and experimental lamellar spacing as a function of position Z = *R** along the droplet diameter D_P passing through the nucleation center. The lamellar spacing λ of the undulated and regular eutectics was measured by a mean intercept method along arcs of circles centered on the nucleation center N (Figure 5). The spacing of the undulated eutectic was found to be constant over zone A at 0.35 ± 0.03 µm. In zone B, λ clearly varies along the growth direction.

The model predicts a small and almost constant lamellar spacing for zone A, followed by a sharp increase in spacing towards the end of recalescence, which represents the transition from zones A to B. The spacing then reaches a maximum in zone B before decreasing again near the end of solidification. The predicted spacing in zone A is similar regardless of the heat transfer approximation used (~0.02 µm). This suggests that growth during recalescence is independent of the mode of heat extraction, i.e. solidification occurs under quasi-adiabatic conditions. However, the simulated eutectic spacing is an order of magnitude lower than what is observed experimentally. Two possible explanations might explain this difference. It could be either due to coarsening induced by the release of latent heat during recalescence and subsequent remaining time of solidification of zone B, or to the growth kinetics of the undulated eutectic which would not follow the well-established kinetic of regular lamellar eutectics. Preliminary experimental results favor the former explanation, but further investigation on that point is ongoing. On the other hand, the behavior of zone B is well represented and can be explained as follows. As the temperature of the droplet increases, the undercooling of the front decreases. The growth velocity decreases and in turn the spacing increases. Towards the end of solidification, the solid-liquid interface S_{sl} decreases (see Figure A.2 in Annex A) and so does the latent heat release. The droplet temperature thus starts to decrease again, increasing the undercooling of the front and thus the velocity of the front v^*. The post-recalescence behaviour (zone B) is affected by the different simulation conditions, with the faster solidification rates leading to smaller eutectic lamellar spacing. In this case, the Whitaker correlation with all

properties taken at the ambient gas temperature shows the best agreement with the experimental values.

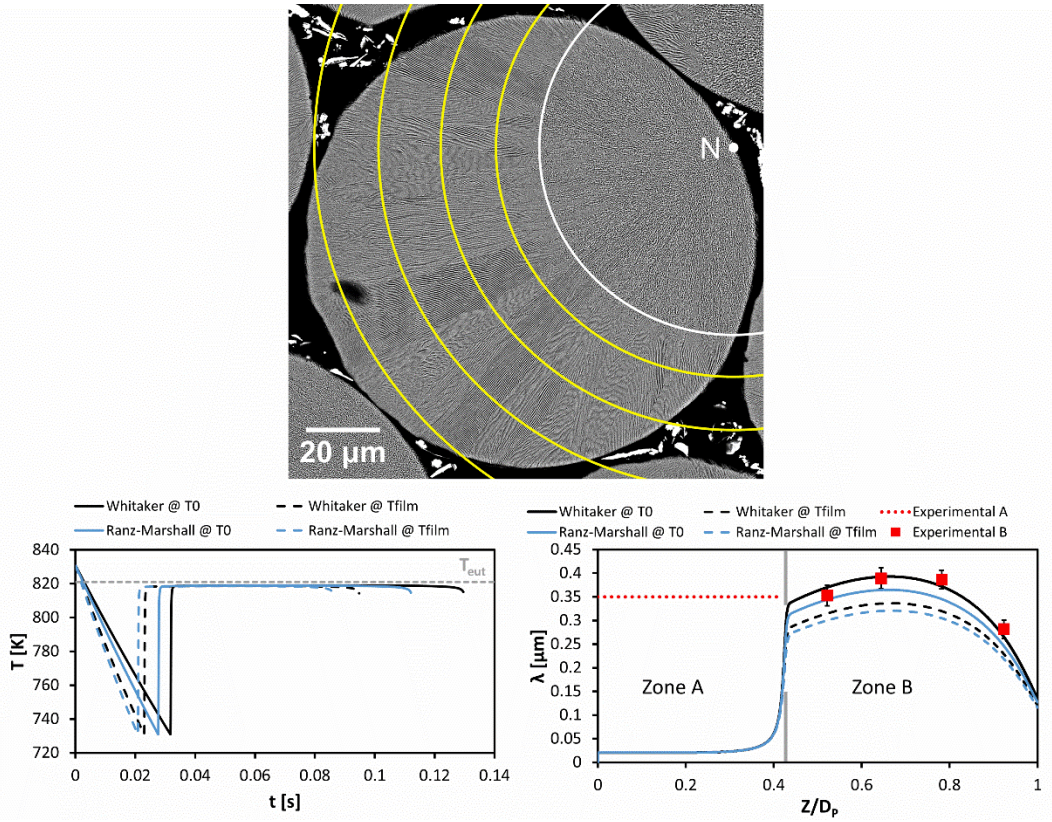

Figure 5: Top: Cross-section of a 123 µm Al-33wt%Cu droplet. The nucleation point N denotes the center of zone A corresponding to $Z = 0$. Assuming spherical growth from the nucleation point, the yellow circles outline various positions of the solid-liquid front along which the lamellar spacing was measured. Left: Modeled temperature profiles with different correlations. Right: Predicted (lines) and measured (dashed red line for zone A and red squares for zone B) lamellar spacing as a function of the solid-liquid interface position $Z = R^*$, normalized by the droplet diameter D_P. The grey line represents the position of the transition between zones A and B.

Figure 6 shows similar experimental and modelling results for a 425 µm diameter droplet. The volume fraction of the undulated eutectic is $g_A \approx 0.20$ in this case, corresponding to an undercooling ΔT_n of about 85 K. For the smaller 123 µm droplet, taking the gas properties at the film temperature led to the shortest solidification times. For the larger particle size, the two fastest growths occur both with the Ranz-Marshall correlation. Conversely, larger eutectic spacing are predicted with the Whitaker correlation. The best fit is found using Whitaker with gas properties taken at the film temperature. This is the case for all particles that were measured with diameters greater than 425 µm. For smaller particles (<300 µm), Whitaker with properties taken at the ambient temperature gave the best agreement with measured lamellar

spacings (note that no experimental results were available for particles between 300 and 425 µm).

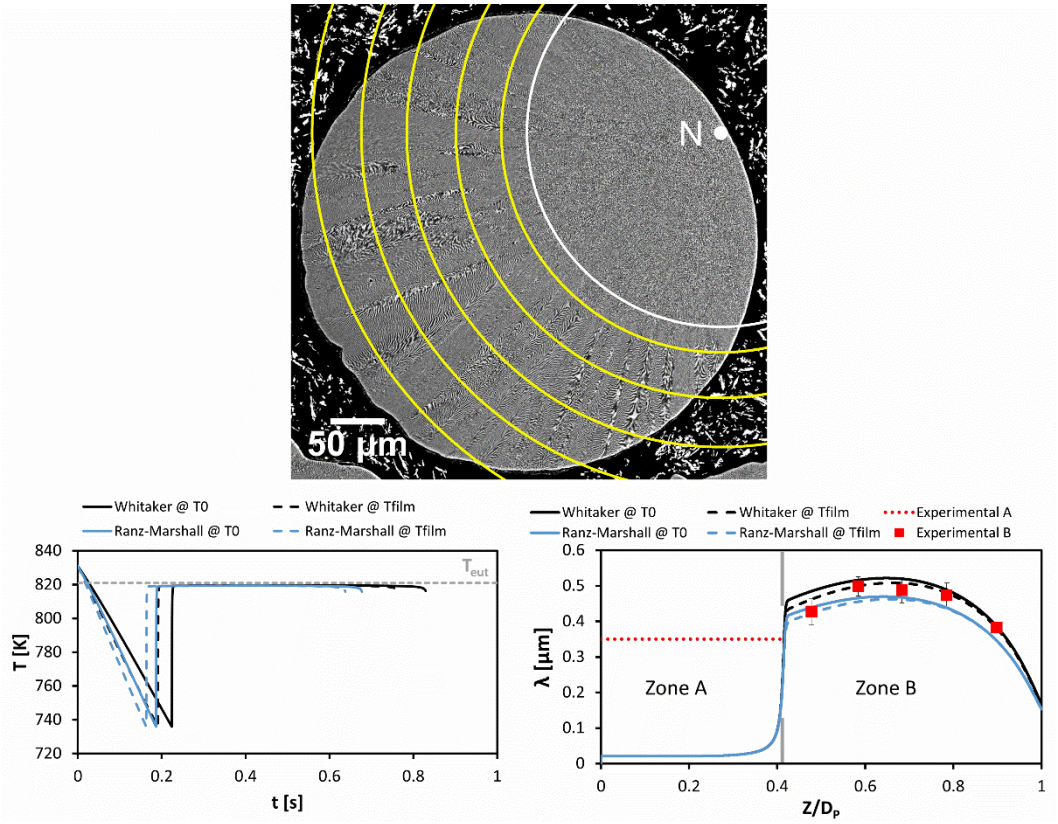

Figure 6: Top: Cross-sections of a 425 µm Al-33wt%Cu droplet. The nucleation point N denotes the center of zone A ($Z = 0$). Left: Modeled temperature profiles with different correlations. Right: Predicted (lines) and measured (dashed red line for zone A and red squares for zone B) lamellar spacing as a function of the solid-liquid interface position $Z = R^*$, normalized by the droplet diameter D_P. The red line represents the position of the transition between zones A and B.

Figure 7 (left) displays the power extracted by the surrounding gas (left hand side of Eq. 2) and the power generated by the release of latent heat during solidification (second term on the right hand side of Eq. 2) for a 159 µm diameter particle. As can be seen, the droplet itself absorbs most of the large amount of latent heat released during recalescence and the external cooling plays a minor role. Once the temperature of the growth front gets close to the eutectic temperature, the power associated with latent heat release decreases drastically and becomes of the same order of magnitude as the power extracted by the surrounding gas. The post-recalescence growth then depends strongly on the heat extraction at the droplet surface. This is reflected in the predicted lamellar spacings in Figure 5 and Figure 6. The heat extracted from the surface and the latent heat release were then integrated over the recalescence period, which for practical purpose was considered to extend from the nucleation temperature up to the temperature at which the volume fraction corresponds to the measured fraction g_A. Figure 7 (right) shows the ratio of the integrated heat extracted over the integrated heat generated as

a function of particle size. For particles diameters between 50 and 650 µm, the heat generated by the growth of the solid during recalescence is one to two orders of magnitude larger than the heat extracted by the surrounding gas. This confirms the quasi-adiabatic conditions during the solidification of zone A. For smaller droplet sizes, the surface-to-volume ratio increases significantly and the conditions are no longer quasi-adiabatic, i.e. the heat generated during recalescence becomes comparable to the heat extraction at the surface of the droplet. For larger particle sizes, the nucleation undercooling decreases, and so do the velocity of the interface and the fraction of solid formed during recalescence. The droplets almost completely solidify at a temperature close to the eutectic temperature without formation of an undulated eutectic.

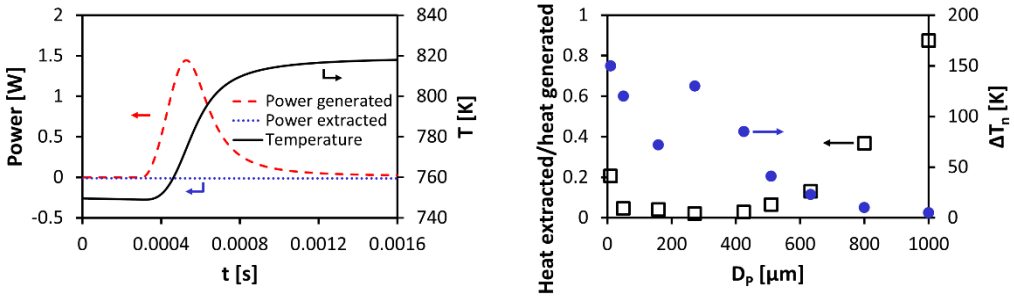

Figure 7: Left: Power generated by the release of latent heat and power extracted by the surrounding gas during the recalescence period of a 159 µm diameter particle. Right: Calculated ratios of the heat extracted from the droplet surface over the heat generated within the droplet during the recalescence period (squares) and measured nucleation undercoolings (circles) as a function of particle size.

To further investigate the influence of the nucleation undercooling, the model was run for two different particle sizes for various imposed values of ΔT_n between 25 and 150 K (Figure 8). The validity of the quasi-adiabatic assumption during recalescence appears to be strongly dependent on the nucleation undercooling. Indeed, as the undercooling decreases, the amount of solid formed during recalescence decreases but the rate of heat extraction by the surrounding gas is similar. While most of the heat generated by the growing eutectic front is still transferred into the undercooled liquid, the amount of heat being dissipated in the surrounding gas becomes non-negligible. This effect is exacerbated at smaller particle sizes as the surface-to-volume ratio increases. Thus, one must be careful when estimating the nucleation undercooling from the experimental fraction of undulated eutectic when that fraction is small.

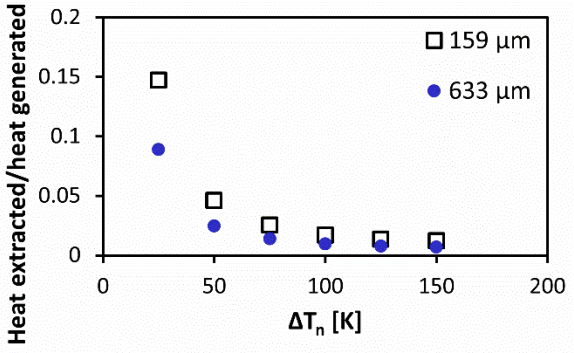

Figure 8: Calculated ratios of the heat extracted from the droplet over the heat generated by the release of latent heat during the recalescence period, as a function of the nucleation undercooling.

5. Conclusions

Rapid solidification of Al-33wt%Cu droplets formed by impulse atomisation revealed two different morphologies: an undulated eutectic that was assumed to develop during recalescence from a nucleation point located at the surface of the droplet, followed by a transition to a lamellar regular eutectic. The eutectic spacing measured in zone A is nearly constant while it varies during growth in zone B. A model of eutectic solidification coupled with an overall heat balance was developed to interpret these experimental results. Two key assumptions were made. First, it was assumed that zone A formed during recalescence, thus allowing to deduce the nucleation undercooling. Second, the growth kinetics of both the undulated and regular eutectics were supposed to be the same and given by scaling laws experimentally established for α-Al-Al_2Cu eutectic [20], [21].

The predicted spacing in zone A is nearly constant, almost independent of the boundary conditions imposed at the surface of the droplets, i.e. eutectic growth during recalescence is independent of the heat transfer coefficient. This confirms the adiabatic nature of solidification during recalescence. However, while the predicted volume fraction of the undulated eutectic is close to the measured values, the lamellar spacing calculated with the model is much smaller than the average spacing measured in zone A. It should be emphasized that this undulated eutectic does not look like a 1-λ or 2-λ oscillating eutectic [20], [22], [23]. While it could be the result of a special, yet unclear growth mode of the α and θ phases with a specific growth kinetics, this undulated eutectics exhibits some faceting which rather suggests that it could be due to a coarsening mechanism occurring in the solid state in order to minimize the (anisotropic) interfacial energy between α and θ. New experimental evidences seem to favor this last explanation but need further investigations and calculations.

The transition from zone A to zone B, i.e. from undulated to regular-lamellar eutectics, is very sharp and the post-recalescence growth of the lamellar eutectic occurs at a temperature much closer to the eutectic temperature. The growth speed is drastically reduced, thus increasing the predicted lamellar spacing which becomes very close to the measured one. In this regime, it is possible to adjust the heat transfer coefficient so as to have the best agreement between measured and predicted spacings. In other words, the lamellar spacing of the regular eutectic is a signature of the heat transfer between the droplet and the surrounding gas. The Whitaker correlation with all gas properties taken at the ambient temperature shows the best agreement with the experimental values for smaller droplets (< 300 µm), while the Whitaker correlation with all properties taken at the film temperature gives the best fit for larger particles (> 425 µm). Smaller droplets do not significantly affect the temperature of the surrounding gas, while larger ones do. Therefore, a universal approach for calculating the heat transfer between a solidifying alloy droplet and the gas phase is to use the Whitaker correlation with the film temperature for large droplets and the gas temperature for small droplets.

Acknowledgment

Financial support from the Natural Sciences and Engineering Research Council of Canada (NSERC) and the Holistic Innovation in Additive Manufacturing (HI-AM) Network is gratefully acknowledged.

References

[1] H. Henein, “Single fluid atomization through the application of impulses to a melt,” *Mater. Sci. Eng. A*, vol. 326, no. 1, pp. 92–100, 2002.

[2] P. Delshad Khatibi, A. B. Phillion, and H. Henein, “Microstructural investigation of D2 tool steel during rapid solidification,” *Powder Metall.*, vol. 57, no. 1, pp. 70–78, Feb. 2014, doi: 10.1179/1743290113Y.0000000072.

[3] W. Hearn, A.-A. Bogno, J. Spinelli, J. Valloton, and H. Henein, “Microstructure Solidification Maps for Al-10 Wt Pct Si Alloys,” *Metall. Mater. Trans. A*, vol. 50, no. 3, pp. 1333–1345, 2019.

[4] J. Valloton, A.-A. Bogno, H. Henein, D. M. Herlach, and D. Sediako, “Scandium Effect on Undercooling and Dendrite Morphology of Al-4.5 Wt Pct Cu Droplets,” *Metall. Mater. Trans. A*, vol. 50, no. 12, pp. 5700–5706, 2019.

[5] K. A. Jackson and J. D. Hunt, “Lamellar and Rod Eutectic Growth,” *Trans. Metall. Soc. AIME*, vol. 236, pp. 1129–1142, 1966.

[6] C. G. Levi and R. Mehrabian, “Heat Flow during Rapid Solidification of Undercooled Metal Droplets,” *Metall. Trans. A*, vol. 13, no. 2, pp. 221–234, Feb. 1982, doi: 10.1007/BF02643312.

[7] H. Kramers, “Heat transfer from spheres to flowing media,” *Physica*, vol. 12, no. 2, pp. 61–80, Jun. 1946, doi: 10.1016/S0031-8914(46)80024-7.
[8] G. C. Vliet and G. Leppert, “Forced convection heat transfer from an isothermal sphere to water,” *J. Heat Transf.*, vol. 83, no. 2, pp. 163–175, 1961.
[9] W. E. Ranz and W. R. Marshall, “Evaporation from drops,” *Chem. Eng. Prog.*, vol. 48, no. 3, pp. 141–146, 1952.
[10] S. Whitaker, “Forced convection heat transfer correlations for flow in pipes, past flat plates, single cylinders, single spheres, and for flow in packed beds and tube bundles,” *AIChE J.*, vol. 18, no. 2, pp. 361–371, 1972.
[11] N. N. Sayegh and W. H. Gauvin, “Numerical analysis of variable property heat transfer to a single sphere in high temperature surroundings,” *AIChE J.*, vol. 25, no. 3, pp. 522–534, 1979, doi: https://doi.org/10.1002/aic.690250319.
[12] J. D. Jackson and J. C. Hatchman, “Measurement of the thermal resistance of paint coatings using a simple transient cooling method,” *Proc. Inst. Mech. Eng. Part J. Power Energy*, vol. 213, no. 1, pp. 45–56, Feb. 1999, doi: 10.1243/0957650991537428.
[13] N. Ellendt, A. M. Lumanglas, S. I. Moqadam, and L. Mädler, “A model for the drag and heat transfer of spheres in the laminar regime at high temperature differences,” *Int. J. Therm. Sci.*, vol. 133, pp. 98–105, Nov. 2018, doi: 10.1016/j.ijthermalsci.2018.07.009.
[14] J. B. Wiskel, H. Henein, and E. Maire, “Solidification Study of Aluminum Alloys using Impulse Atomization: Part I: Heat Transfer Analysis of an Atomized Droplet,” *Can. Metall. Q.*, vol. 41, no. 1, pp. 97–110, 2002.
[15] J. B. Wiskel, K. Navel, H. Henein, and E. Maire, “Solidification Study of Aluminum Alloys Using Impulse Atomization: Part ii. Effect of Cooling Rate on Microstructure,” *Can. Metall. Q.*, vol. 41, no. 2, pp. 193–204, 2002.
[16] M. Zimmermann, “Solidification rapide de l’eutectique Al-Al2Cu par refusion laser,” PhD thesis, Ecole Polytechnique Fédérale de Lausanne, Lausanne, 1990.
[17] J. R. Welty, C. E. Wicks, and R. E. Wilson, *Fundamentals of Momentum, Heat and Mass Transfer*, 3rd ed. New York: John Wiley and Sons, 1984.
[18] R. C. Weast, *CRC Handbook of Chemistry and Physics*, 61st ed. Boca Raton: CRC Press Inc, 1980.
[19] V. A. Rabinovich, V. I. Nedostup, A. A. Vasserman, and L. S. Veksler, *Thermophysical Properties of Neon, Argon, Krypton and Xenon*, 10th ed. USSR, 1988.
[20] J. A. Dantzig and M. Rappaz, *Solidification*. Lausanne: EPFL Press, 2009.
[21] H. Jones, *Rapid solidification of metals and alloys*. London: Institution of Metallurgists, 1982.
[22] S. Akamatsu, G. Faivre, and S. Moulinet, “The formation of lamellar-eutectic grains in thin samples,” *Metall. Mater. Trans. A*, vol. 32, no. 8, pp. 2039–2048, Aug. 2001, doi: 10.1007/s11661-001-0016-y.
[23] S. Akamatsu, G. Faivre, M. Plapp, and A. Karma, “Overstability of lamellar eutectic growth below the minimum-undercooling spacing,” *Metall. Mater. Trans. A*, vol. 35, no. 6, pp. 1815–1828, Jun. 2004, doi: 10.1007/s11661-004-0090-z.

Appendix A

This appendix details the relationship between the volume V_s and the radius R^* of the solid formed in a droplet from a nucleation point located at the surface. A spherical particle of radius R_p and volume V_P is considered. The solid is assumed to be a sphere of radius R^*, nucleated on the surface of the particle (Figure A.1). The growth velocity v^* is considered to be uniform over the solid-liquid interface. At any instant, the solid is made of two spherical caps: V_α of radius R^* and V_β of radius R_p, with cap angles α and β respectively, so that $V_s = V_\alpha + V_\beta$.

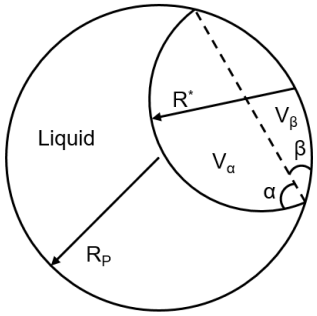

Figure A.1: Schematic view of the geometry considered.

Simple geometric arguments show that:

$$\cos\alpha = \frac{R^*}{2R_P} \tag{i}$$

$$\cos\beta = 1 - 2\sin^2\frac{\beta}{2} = 1 - \frac{1}{2}\left(\frac{R^*}{R_P}\right)^2 \tag{ii}$$

The volume of the spherical caps are expressed as follows:

$$V_\alpha = \frac{4}{3}\pi R^{*3}\frac{(1-\cos\alpha)^2(2+\cos\alpha)}{4} = \frac{4}{3}\pi R^{*3} f(\alpha) \tag{iii}$$

$$V_\beta = \frac{4}{3}\pi R_P^3\frac{(1-\cos\beta)^2(2+\cos\beta)}{4} = \frac{4}{3}\pi R_P^3 f(\beta) \tag{iv}$$

The growth of the solid is then given by:

$$\left(\frac{1}{V_P}\right)\frac{dV_S}{dt} = \left(\frac{1}{V_P}\right)\frac{dV_S}{dR^*}v^* \tag{v}$$

with:

$$\left(\frac{1}{4\pi R_P^2}\right)\frac{dV_S}{dR^*} = \left(\frac{R^*}{R_P}\right)^2 f(\alpha) + \left(\frac{R^*}{R_P}\right)^3 \frac{(\cos^2\alpha) - 1}{8} - \frac{R^*}{R_P}\frac{(\cos^2\beta) - 1}{4} \quad \text{(vi)}$$

The evolution of the normalized solid volume $\frac{V_S}{V_P}$ and normalized effective surface $\left(\frac{1}{4\pi R_P^2}\right)\frac{dV_S}{dR^*}$ as a function of the normalized particle radius $\frac{R^*}{R_P}$ is given in Figure A.2 over the whole droplet diameter.

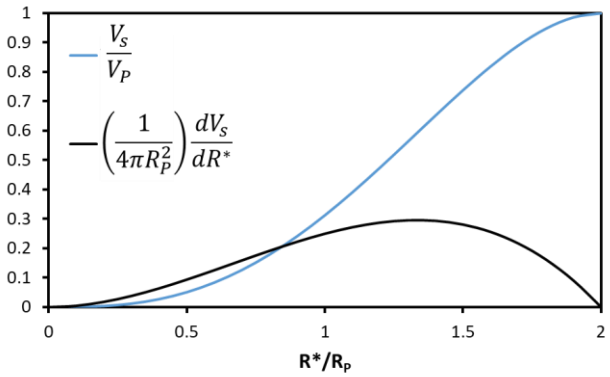

Figure A.2: Evolution of $\frac{V_S}{V_P}$ and $\left(\frac{1}{4\pi R_P^2}\right)\frac{dV_S}{dR^*}$ as a function of $\frac{R^*}{R_P}$.